Chapter

Biomass-Based Carbon Electrodes in the Design of Supercapacitors: An Electrochemical Point of View

Antony Bazan-Aguilar, Elvis O. López, Miguel Ponce-Vargas and Angélica M. Baena-Moncada

Abstract

The urgent demand of sustainable long-lasting batteries has fostered the improvement of extended-use technologies e.g., Li-ion batteries, as well as the development of alternative energy storage strategies like supercapacitors. In this context, new carbon-based materials were developed to attain higher electrochemical performances, even though several of these materials are not obtained by eco-friendly methods and/or in a considerable amount for practical purposes. However, up-to-date reports stand out the scopes achieved by biomass-based carbon materials as energy storage electrodes combining outstanding physicochemical and electrochemical properties with low-pollutant and low-cost production. On this basis, this chapter will expose several aspects of the synthesis of carbon-based electrodes from biomass, focusing on the influence of their surface properties: porosity, crystallinity, and morphology on their electrochemical performance in supercapacitors.

Keywords: Biomass-based carbon electrodes, Energy storage device, Surface properties, Electrochemical performance, Supercapacitors

1. Introduction

Nowadays, the search for new eco-friendly energy systems is a priority to mitigate the global impact associated with fossil fuel energy consumption [1–4]. At the same time, novel electronic devices need to be developed to produce more efficient energy storage systems with higher capacity and longer average lifetimes [5]. In this regard, electrical double layer capacitors (EDLC), pseudocapacitors [6] and flexible solid-state supercapacitors (FSSC) [7, 8], are able to cover the above-mentioned demands. Particularly, carbon-based capacitors exhibit significant advantages, such as high-power density, low weight and flexibility, in contrast to conventional graphite-based systems [9]. To achieve a better capacitance, electrodes based in porous carbon materials can be employed, given their interesting morphological features, like high specific surface area (S_{BET}), defined-porosity, and hierarchical arrangement [10]. Recently, the use of biomass as precursor material has allowed the design of carbon-based energy storage systems with outstanding electrochemical and mechanical properties [11, 12].

The energy storage mechanism in these materials consists in the accumulation of electrostatic charges on their surface (**Figure 1**), [13] implying that, density of stored charges depends on the material morphology (roughness and pores), and the size of the

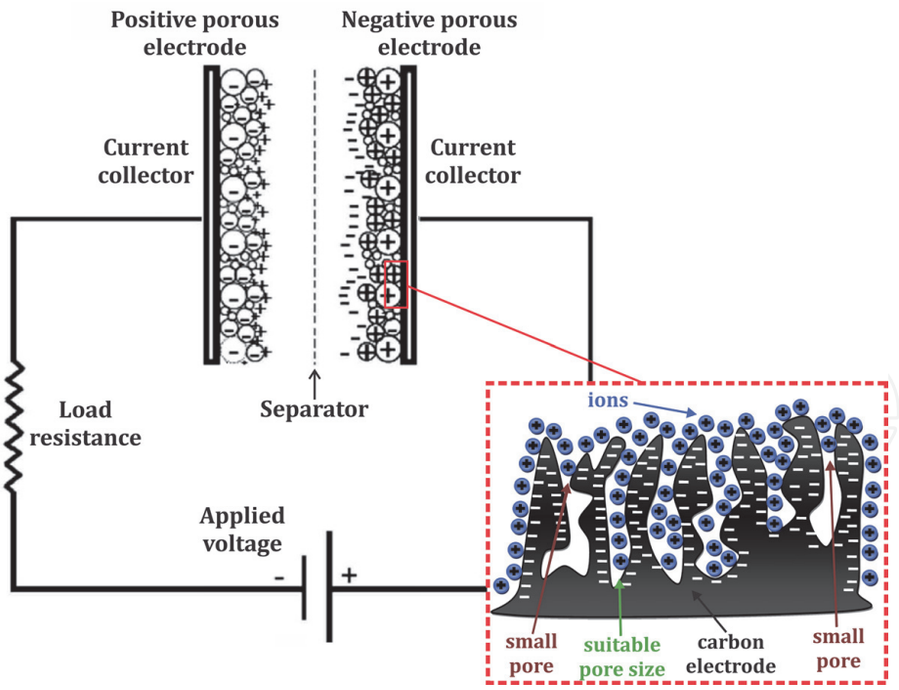

Figure 1.
Schematic representation of a loaded EDLC supercapacitor and pore accessibility (inset) with respect to the electrolyte. Figure adapted from [13, 14].

involved electrolyte ions [14]. **Figure 1** shows the interplay between electrode porosity and ion-electrolyte size for the electrostatic charge accumulation, in terms of pore accessibility. In this way, activated carbons mainly exhibit three pore sizes [15]: micro (< 2 nm), meso (2–50 nm) and macro (> 50 nm), being the micropores and mesopores the ones that most contribute to the increase of the capacitance [16]. Nevertheless, even though carbon-based materials have high surface areas (1000–2000 $m^2 g^{-1}$), they still have low specific capacitances due to their limited mesoporosity [14].

The carbons from biomass can be obtained from various natural sources, such as: garlic skin, bamboo, rice husk, eucalyptus-bark, lignin, cellulose, orange peel, etc. [6, 17–22], making biomass a sustainable source, also available in large quantities from industrial waste [18]. Furthermore, the carbons obtained from biomass present a diversified class of fibrous and porous structures [22], with capacitances ranging from 100 to 430 F g^{-1} [16, 23]. However, these values vary according to the carbon activation method, which is strongly related to the resulting electrode pore-size. Such processes of carbon activation from biomass can be divided into two categories: i) physical activation and ii) chemical activation.

1.1 Physical activation processes

In this process the biomass undergoes a pyrolysis treatment at temperatures between 600 and 900°C in inert atmosphere. Then, the material is commonly exposed to an oxidizing atmosphere of CO_2, carried out at temperatures between 600 and 1200°C. Yu et al. used this method to obtain activated carbon from cattail biomass [24], resulting in an activated carbon with a surface area of 441 $m^2 g^{-1}$ and a specific capacitance of 126 F g^{-1} (current density of 0.5 A g^{-1} in KOH 6 mol L^{-1} electrolyte) [18].

1.2 Chemical activation processes

In this process, the carbon precursor (biomass) is treated (soaked) with chemical activators, such as: KOH, NaOH, H_3PO_4, $ZnCl_2$, H_2SO_4, among others.

Subsequently, the biomass is carbonized at temperatures between 400 and 900°C [25]. During this activation, redox processes and substitution of large particles take place, leading to the desired high porosity. In addition, physical activation occurs due to the interaction of the reaction products such as: H_2, H_2O, CO and CO_2. Remarkably, these molecules also contribute to the pore formation.

Using KOH as a chemical activator, K^0 (metallic) is produced which occupies interstitial positions in the carbon structure, inducing expansion in the material as well as producing a high microporosity. A proposed mechanism of the activation process using KOH is shown in the following redox reactions [26]:

$$6KOH + 2C \rightarrow 2K + 3H_2 + 2K_2CO_3 \quad (1)$$

$$2K_2CO_3 \rightarrow 2K_2O + 2CO_2 \quad (2)$$

$$K_2CO_3 + 2C \rightarrow 2K + 3CO \quad (3)$$

$$CO_2 + C \rightarrow 2CO \quad (4)$$

$$C + K_2O \rightarrow 2K + CO \quad (5)$$

Diverse works have used the chemical activation process from KOH, Barzegar et al. was one of them and produced mesoporous carbon from coconut shell, obtaining a specific surface area of 1416 $m^2\ g^{-1}$ and a specific capacity of 186 F g^{-1} [27]. Zhang et al. used bamboo to obtain mesoporous carbon from KOH as an activator. Zhang obtained a high specific surface area of 2221 $m^2\ g^{-1}$ and a specific capacitance of 293 F g^{-1} at 0.5 A g^{-1} in KOH 3.0 mol L^{-1} [18]. Yin et al. produced activated carbon from coconut fibers with KOH as a chemical activator. This product exhibits a surface area of 2898 $m^2\ g^{-1}$ (pore volume of 1.59 $cm^3\ g^{-1}$, i.e. 30% of mesoporosity) and specific capacitance of 266 F g^{-1} at 0.1 A g^{-1} in KOH 6.0 mol L^{-1} [28]. Another biomass used to produce activated carbon is the garlic skin activated with KOH, this material presents a surface area of 2818 $m^2\ g^{-1}$, exhibiting excellent electrochemical performance and cycle stability at a current density of 0.5 A g^{-1} (specific capacitance of 427 F g^{-1} or 162 F cm^{-3}) and a retention capacitance of 94% [17].

Remarkably, the use of H_3PO_4 as activator leads to a lower surface area in comparison to those obtained using KOH or $ZnCl_2$. It implies a controlled porosity in the mesopore range. The addition of H_3PO_4 activator also enables to obtain surfaces composed of different functional groups such as quinones and phosphide groups -C-O-P-, which subsequently decompose into CO at ~ 860°C. In addition, with this activation type, large capacitance values can be obtained, all due to the nature of the phosphorus functional groups in the carbon structure [23].

Another source of biomass as coconut was also activated using NaOH. In this case, Sesuk et al. showed that the carbon material presented a surface area of 2056 $m^2\ g^{-1}$ and specific capacitance of 192 F g^{-1} at 1.0 A g^{-1} [29].

Orange peels in copper carbonate ($CuCO_3$) were also used to produce activated carbon. These materials present a surface area of 912 $m^2\ g^{-1}$ and specific capacitance of 375 F g^{-1} (current density of 1.0 A g^{-1}) [22].

Among the great variety of surface functional groups able to be incorporated on the material surface we can mention: OH^-, $COOH^-$, CO, as well as adsorbed molecules [25]. These functional groups increase their electron affinity in the aqueous medium, inducing electrochemical reactions [26, 30], which shows that their specific capacitance could be improved by addition of a pseudocapacitive component due to reversible faradaic redox involved in this type of molecules. In **Figure 2**, the optimized structures of 2,7-dimehtyl-9,10-phenanthrenequinone and its reduced form, adsorbed on a graphene surface obtained by density functional

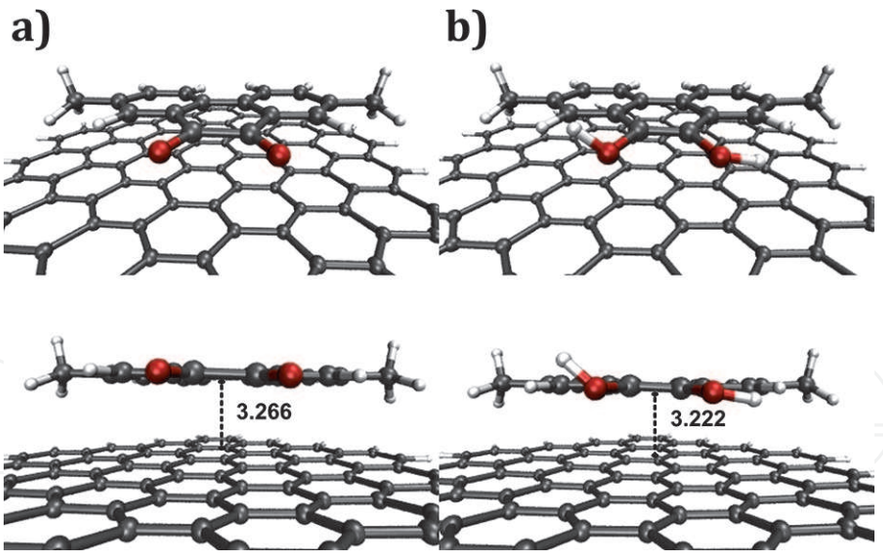

Figure 2.
Optimized structures of 2,7-dimehtyl-9,10-phenanthrenequinone (a) and its reduced form (b) adsorbed on a graphene surface, at the M06-2X/6-311G(d,p) level of theory. Distances in Angstroms.

theory (DFT) calculations at the M06-2X/6-311G(d,p) level of theory, are presented.

2. Reduced graphene oxide modified carbon Fibers

In the search for a low-cost electrode, with large surface area and optimal charge retention capacity, it has been found that carbon fiber or cotton exhibits adequate surface area properties and mechanical and electrochemical stability, in comparison with other porous carbon-based electrodes [31]. Certainly, different authors have reported that the micro and macro-porosity are formed during the lignite carbonization on cotton, but the tubular structure of the cellulose fibers is not altered in the pyrolysis process [32]. In this way, carbon cotton electrodes present a large surface area related to its micro and macro-porosity [31]. Another advantage linked to the production of these electrodes is the low cost and ease synthesis, *e.g.* Sheng-Heng et al. have reported commercial cotton carbonization at 900°C under Ar atmosphere for 6 h, with area of 805 $m^2\ g^{-1}$ and average micropore size of 1 nm [33]. On the other hand, H. Wang et al. have obtained activated cotton carbons from cotton pieces treated with solution of KOH-H_2O or KOH-urea-H_2O at 700°C for 2 h under N_2 atmosphere. These activated cotton carbons show 1286 $m^2\ g^{-1}$ of surface area and high electrochemical stability after several charge–discharge cycles as cathode in Li-S batteries [31].

In previous studies, the influence of reduced graphene oxide (r-GO) on carbon cloths and its capacity to charge store and stability have been studied. The carbonization of cotton fibers impregnated with graphene oxide at 1000°C for 2 h shows a reversible charge–discharge behavior of 160 mA h g^{-1} after 100 cycles [34]. In contrast, the design of carbon fiber material doped with nitrogen reports an outstanding stability after 200 charge–discharge cycles at 1 A h g^{-1} [34–36]. To a better understanding of modified carbon cotton cloths with r-GO on electrochemical performance, carbon cotton cloths were synthetized with r-GO 3 mg mL^{-1}, and the effect of inert atmosphere was evaluated. To achieve this, commercial cotton fibers were impregnated with graphene oxide (GO) during 0, 15, 30 and 45 min, after dried at 60°C the samples were pyrolyzed at 800°C (3°C min^{-1}) for 30 min under

N_2 or Ar atmosphere to obtain N/CC and N/CC/rGO_{5-45}, or Ar/CC and Ar/CC/rGO_{5-45} electrodes, respectively (**Figure 3**).

According to the EDS analysis, cotton fibers (COT) report a carbon mass percent (% m of C) of 49.1%, which increases to 63.9% after the GO impregnation stage for COT/GO_{45}, presumably due to the presence of GO sheets on the cotton fibers surface. Similarly, after the heat treatment there is a carbon content increment of 95.6% for Ar/CC. This large increase has been associated with the CO bonds breaking during the cellulose fiber polymerization process when it is treated at temperature higher than 400°C [37], but without an apparent alteration of the fibrillary structure. The same behavior is observed for carbonized fibers covered by rGO, with values of 90.7% ($N/CC/rGO_{45}$) and 92.87% ($Ar/CC/rGO_{45}$) of carbon mass (% m of C), suggesting that the reduction of oxygenated groups in COT and the GO is higher under Ar atmosphere (**Table 1**). This implies that the composition, crystallinity, and porosity of carbonaceous electrodes are dependent on the atmosphere used during carbonization. Both N_2-made and Ar-made electrodes have a similar fibrillary structure as seen in **Figure 4a** and **c**. However, at high magnification, it is observed that samples N/CC/rGO_{5-45} and Ar/CC/rGO_{5-45} present a rough surface covered by a porous carbon layer, which would indicate that the rGO sheets were inserted efficiently and independently of the gas used in the heat treatment (**Figure 4b** and **d**). There are marked differences between both systems where samples treated under N_2 atmosphere present a more compact rough surface with a rather scaly appearance (**Figure 4b**). On the other hand, those heat treated under Ar atmosphere show layers of rGO with a laminar appearance around the fiber and regions of homogeneous roughness (**Figure 4d**).

IR spectroscopy permits to elucidate the type and degree of GO-COT, and rGO-carbon fibers (CC) interactions. The main vibrational modes corresponding to the

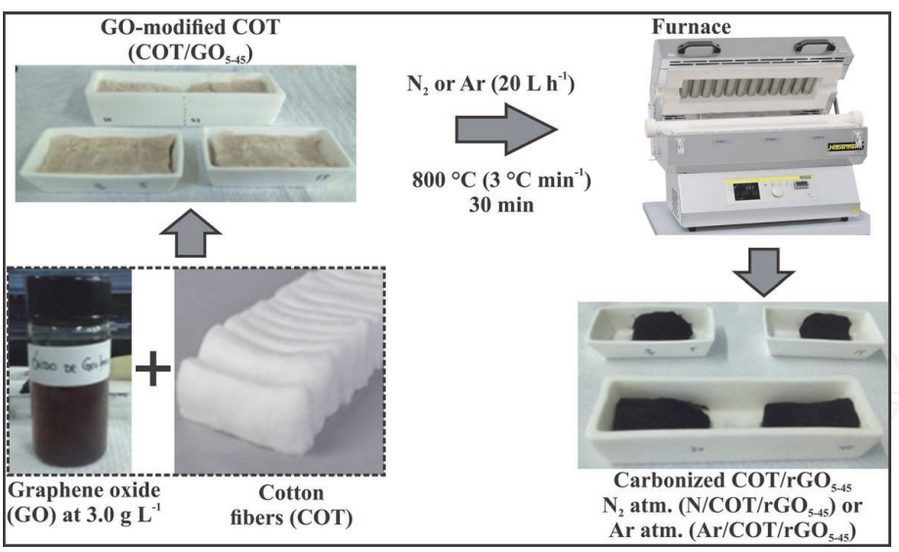

Figure 3.
Schematic diagram of the synthesis of rGO-modified carbonized cotton fibers.

Sample	COT	COT/GO_{45}	N/CC	$N/CC/rGO_{45}$	Ar/CC	$Ar/CC/rGO_{45}$
C mass %	49.1	63.9	93.3	90.7	95.6	92.9
O mass %	50.9	36.1	6.7	9.3	4.4	7.1

Table 1.
Carbon and oxygen mass percent obtained from EDX analysis for COT, COT/GO_{45}, N/CC, Ar/CC and Ar/CC/rGO_{45} samples [38].

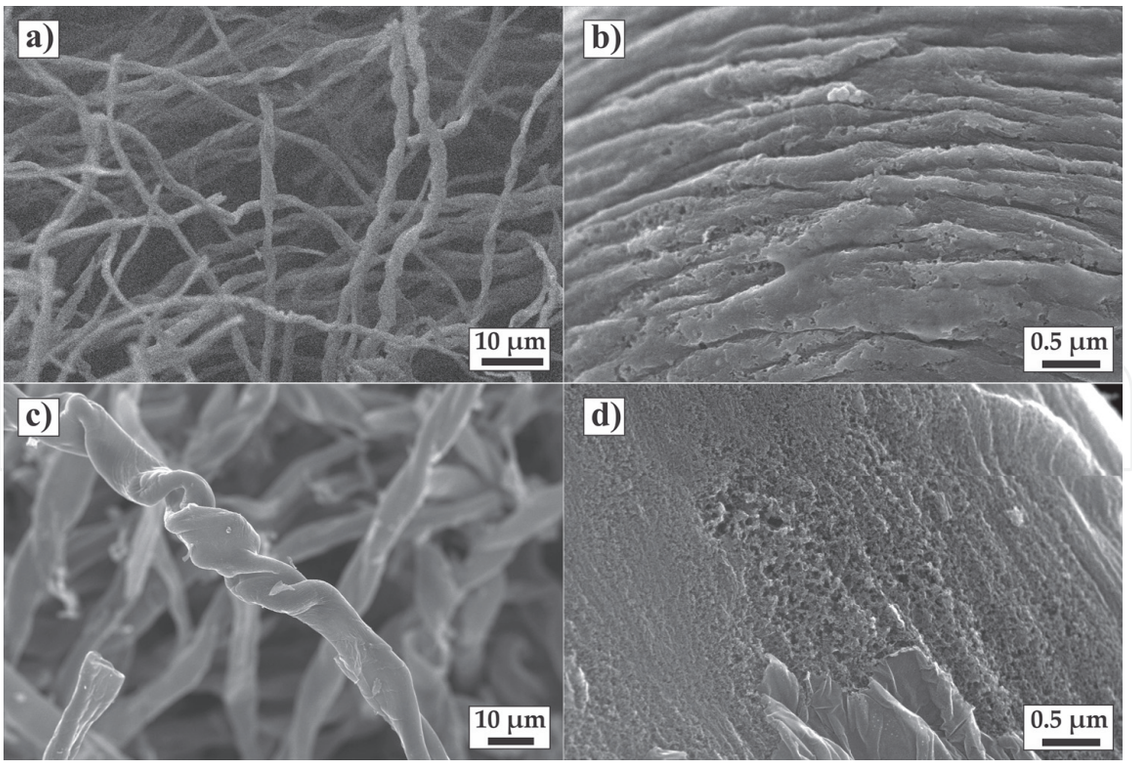

Figure 4.
SEM image of rGO-modified carbonized made fibers made under N_2 atmosphere (a, b) N/CC/rGO$_{45}$, and Ar atmosphere, (c, d) Ar/CC/rGO$_{5\text{-}45}$.

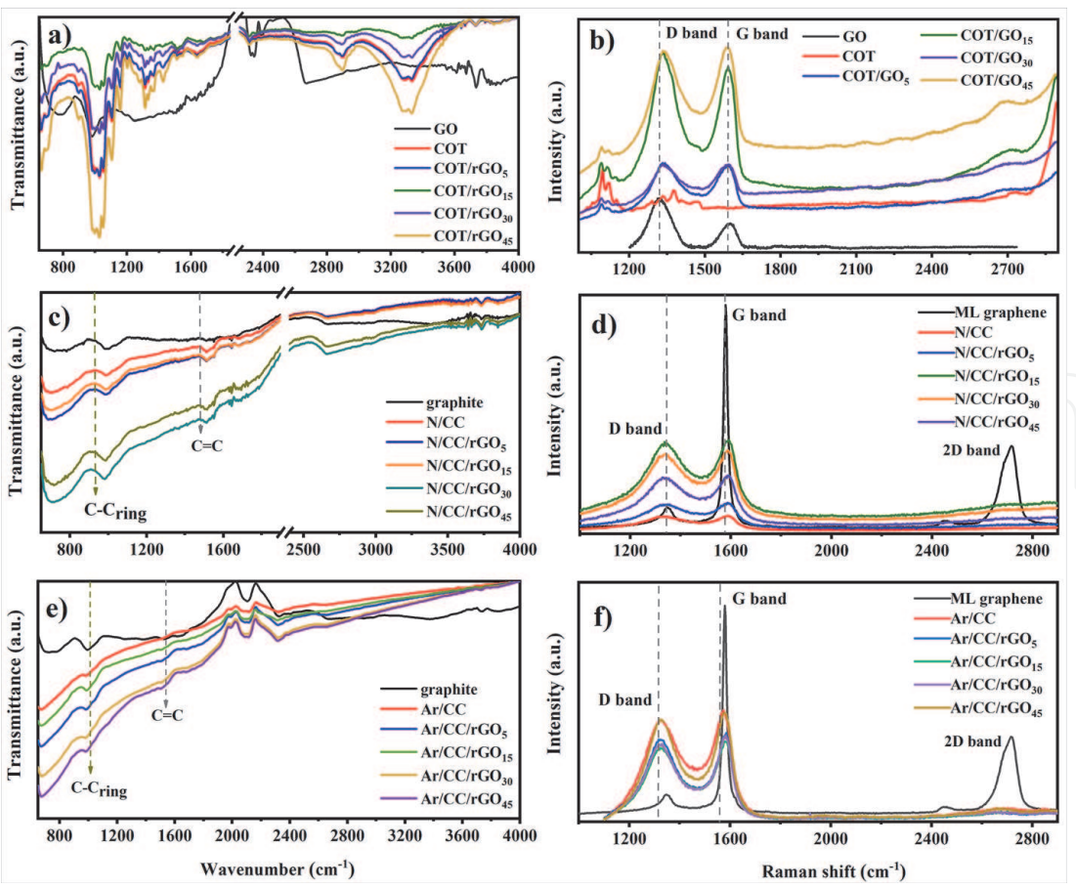

Figure 5.
Infrared and Raman spectra of (a, b) cotton fibers (COT) and GO-covered cotton fibers (COT/GO$_{5\text{-}45}$) and rGO-modified carbonized cotton fibers made under N_2 atm. (N/CC and N/CC/rGO$_{5\text{-}45}$) or Ar atm. (Ar/CC and Ar/CC/rGO$_{5\text{-}45}$). Raman laser source excitation of 532.5 nm.

characteristic chemical bonds present in COT are reported before and after the impregnation (COT and COT/GO_{5-45}) and the carbonization stage (N/CC/rGO_{5-45} and Ar/CC/rGO_{5-45}), respectively (**Figure 5**). After the first stage, it is observed that the chemical groups C=O (1033.8 cm^{-1}), CH_2 (1322.2 cm^{-1}), C=O (1639.5 cm^{-1}), C-H (2893.2 cm^{-1}) and O-H (cellulosic, 3325.3 cm^{-1}) present an intensity reduction which could be correlated with GO layer. This reduction can also be associated with the interaction between the functional groups of GO and cellulose fibers. Since the cellulose OH and C=O groups register a decreasing in their intensities, it can be assumed that there exists a direct interaction between these chemical groups by hydrogen bonds [38]. According to IR spectroscopy, the bands at 979.8 and 1512.2 cm^{-1} are related to C-C_{ring} and C=C bonds, respectively, verifying a certain degree of graphitization. This thermal conversion has been described by M. M. Tang et al. who found that cellulose in cotton fibers undergoes a breakdown of the glycosidic bonds at temperatures above 250°C, allowing the elimination of various CO bonds and the breakdown of several C-C bonds along with a substantial mass loss due to H_2O, CO and CO_2 removal [39]. When the temperature is greater than 400°C, the remaining fractions of C-H hydrocarbon rings start an aromatization stage with H_2 loss and the formation of C=C bonds as part of a carbon polymeric structure [37]. It is observed that the conversion process to a graphitic like structure is similar for N/CC/rGO_{5-45} and Ar/CC/rGO_{5-45} (**Figure 5**).

The analysis of Raman spectra from **Figure 5b, d** and **f** show that N/CC/rGO_{5-45} electrodes present a slight improvement in their crystallinity with respect to the modified cotton fibers, reporting a crystallite size from 19.39 (COT/GO_{30}) to 20.10 nm (N/CC/rGO_{30}), that is, an improvement of 4 to 5% (**Figure 6**). This behavior is also observed in the variation of the defect density from Ar/CC to Ar/CC/rGO_{5-45} and from N/CC to N/CC/rGO_{5-45}.

For instance, Ar/CC/rGO_{30} register 21.9 × 10^{10} defects cm^{-2} compared to N/CC/rGO_{30}, whose value was 21.1× 10^{10} defects cm^{-2} (**Figure 6**). According to Yo-Rhin Rhim et al. the peaks centered at 1620 cm^{-1}, between 1500 to 1550 cm^{-1} and about 1100 cm^{-1}, are associated with ordered π bonds, sp^2 amorphous systems,

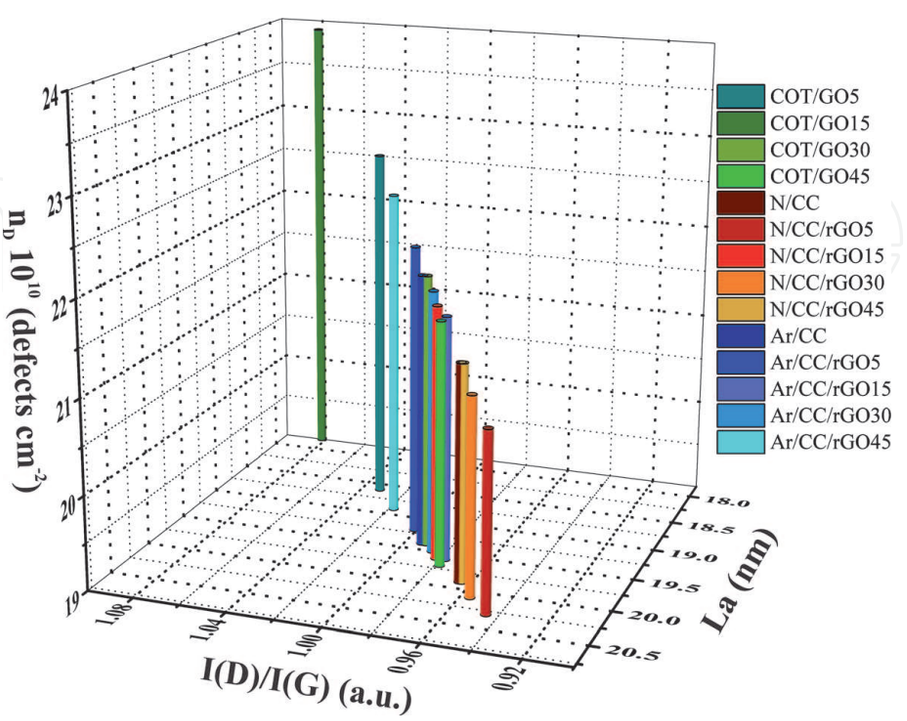

Figure 6.
3D graph of defect density (n_D) as function of I(D)/I(G) ratio and crystallite size (L_a) from Raman spectroscopy analysis.

and sp^3 bonds, respectively. Additionally, the systems under study were treated at 800°C, the restoration of the C=C bonds in the RGO is guaranteed and remains stable inside of the carbon fiber matrix [32]. Similarly, Ar/CC and Ar/CC/$rGO_{5\text{-}45}$ electrodes show a slight increase in crystallite size, for example, Ar/CC/rGO_{30} registered a value of 19.5 nm in contrast to that reported for its precursor COT/GO_{30}, i.e., 19.39 nm (**Figure 6**). Although this variation is small, the effect of the carbonization stage is better appreciated when defect density is compared, e.g., Ar/CC/rGO_{30} shows 21.8× 10^{10} defects cm^{-2} while COT/GO_{30} was 21.9× 10^{10} defects cm^{-2}. This result means that the GO sheets supported on the cotton fibers present an excess of 0.1× 10^{10} defects cm^{-2} compared to Ar/CC/rGO_{30} sample. It can thus be suggested that the nature of the inert atmosphere influences the degree of graphitization of the obtained products. Under N_2 atmosphere, a higher crystallinity is observed in N/CC/rGO_5 with a value equal to 20.3 nm and a defect density of 20.9 × 10^{10} defects cm^{-2}. In the case of cotton fibers modified with GO treated under Ar atmosphere, the optimal registered support is Ar/CC/rGO_{15} with a crystallite size of 19.6 nm and a defect density of 21.6 × 10^{10} defects cm^{-2}.

According to IR and Raman analysis, it is confirmed that GO sheets are intimately impregnated on cotton fibers through O-H or C=O interactions, and this interaction intensifies after the carbonization stage [38]. This effect is corroborated as an increase in crystallinity and a decrease in the density of defects (**Figure 6**). Therefore, through Raman spectroscopy it is possible to elucidate those carbonaceous materials that present a higher degree of crystallinity, lower defect density and higher density of sp^2 carbons which providing a high electrical conductivity. The evidence from these results suggests that samples such as N/CC/rGO_5, N/CC/rGO_{30}, Ar/CC/rGO_5 and Ar/CC/rGO_{30} are shown as promising matrices in the design of supercapacitors.

On the other hand, N_2 adsorption–desorption experiments were used to investigate the surface characteristics of the synthesized samples. It was possible to determine the specific surface area (S_{BET}), the degree and porosity type of the designed materials. In the case of N/CC presents a S_{BET} of 453.3 $m^2\ g^{-1}$, shaped of a microporous area (S_{micro}) of 265.9 $m^2\ g^{-1}$ and with a size pore of 1.99 nm (**Table 2**). Furthermore, N/CC/rGO_{15} and N/CC/rGO_{30} exhibit S_{BET} values of 1221.3 and 1804.8 $m^2\ g^{-1}$, respectively. These values suggest the presence of a highly porous rGO layer on carbonized cotton fibers prepared under N_2 atmosphere. Specifically, a high microporosity of 882.4 and 1350.2 $m^2\ g^{-1}$ is reported for the N/CC/rGO_{15} and N/CC/rGO_{30}, respectively, as a consequence of a large volume of micropores with diameters close to 1.88 nm (N/CC/rGO_{15}) and 1.80 nm (N/CC/rGO_{30}). Similarly, there was an increase in the S_{BET} from 1073.6 to 1457.5 $m^2\ g^{-1}$, but with a substantial increase in mesoporosity from 298.6 to 729.8 $m^2\ g^{-1}$ for the Ar/CC and Ar/CC/

Samples		S_{BET}/ $m^2\ g^{-1}$	S_{micro}/ $m^2\ g^{-1}$	S_{meso}/ $m^2\ g^{-1}$	S_{micro}/S_{meso}	Pore/nm
N_2-made electrodes	N/CC	453	266	187	1.4	2.0
	N/CC/rGO_{15}	1221	882	339	2.6	1.9
	N/CC/rGO_{30}	1805	1350	455	2.9	1.8
Ar-made electrodes	Ar/CC	1074	775	299	2.6	2.1
	Ar/CC/rGO_{15}	1458	728	730	1.0	2.0
	Ar/CC/rGO_{30}	1207	784	423	1.9	2.0

Table 2.
Surface properties registered by N_2 adsorption–desorption experiment [38].

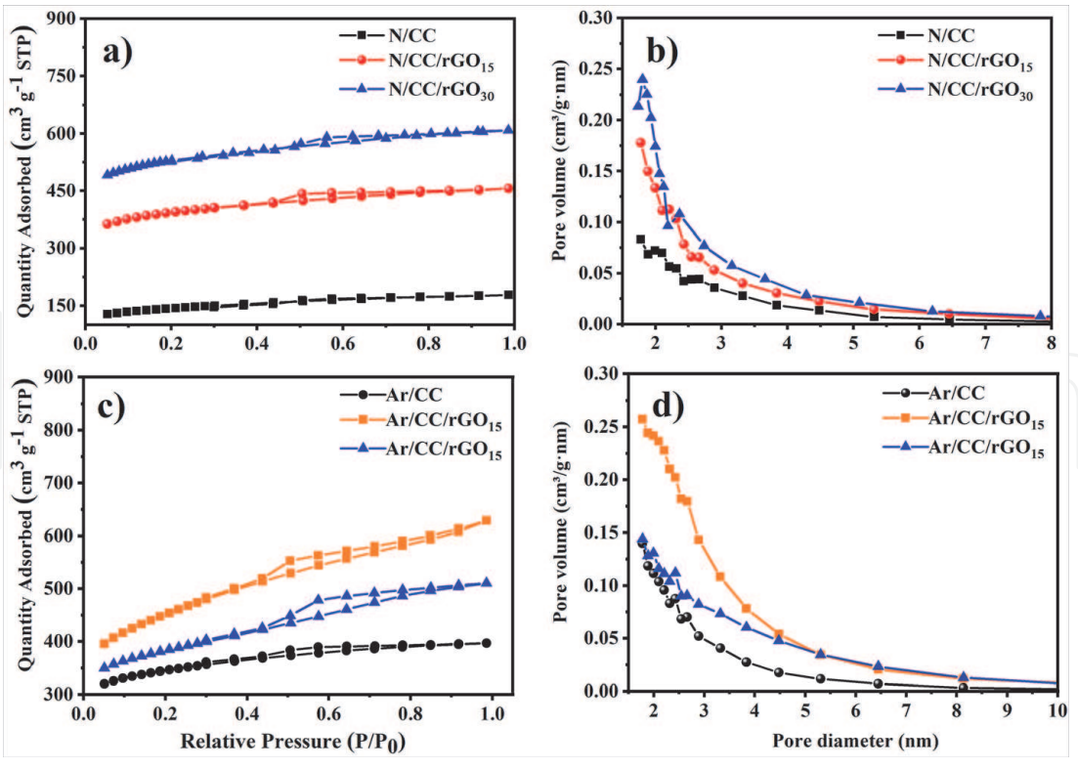

Figure 7.
N_2 adsorption–desorption isotherms and pore size distribution of carbonized cotton fibers made under (a, b) N_2 atmosphere. (N/CC and N/CC/rGO$_{5\text{-}45}$) and (c, d) Ar atmosphere. (Ar/CC and Ar/CC/rGO$_{5\text{-}45}$).

rGO$_{15}$, respectively (**Figure 7c**). Additionally, it was observed that the Ar/CC/rGO$_{15}$ presents a balance between micro and mesoporosity with a ratio of 1: 1, in contrast to Ar/CC (2.6: 1) and Ar/CC/rGO$_{30}$ (1.9: 1). It can therefore be asserted that the electrochemical properties could be modified in the same way and correlated with the aforementioned texture properties [10].

Regarding to cyclic voltammetry test, a layer capacitive profile for N/CC (**Figure 8a**), Ar/CC, Ar/CC/rGO$_{15}$ and Ar/CC/rGO$_{30}$ (**Figure 8b**) is observed, while an increment of resistivity for N/CC/rGO$_{15}$ and N/CC/rGO$_{30}$ is registered

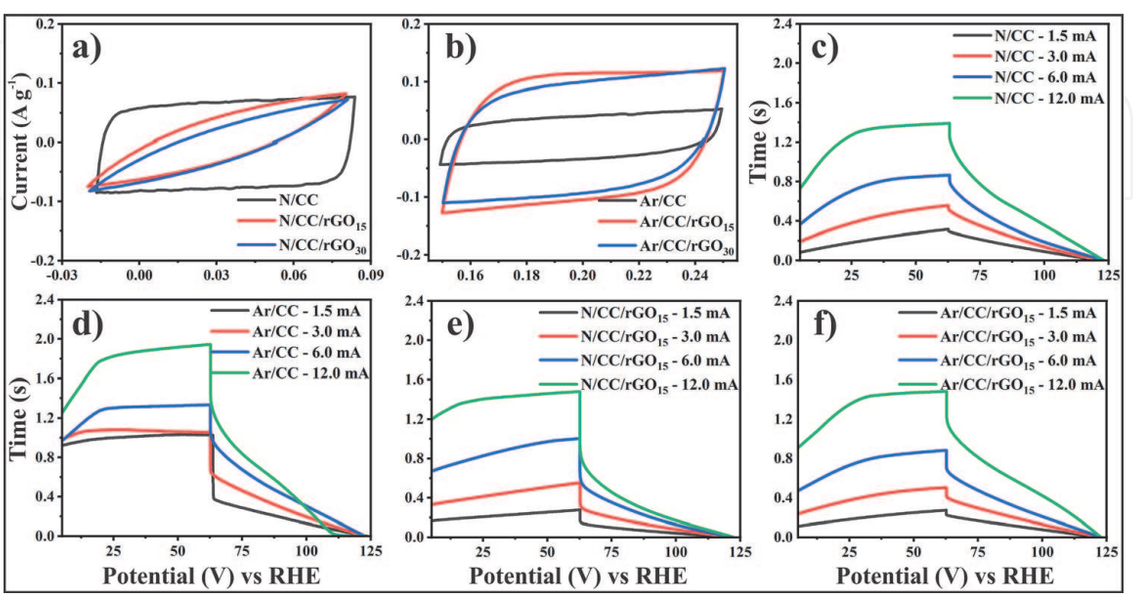

Figure 8.
Cyclic voltammetry of (a) N/CC, N/CC/rGO$_{15}$ and (b) Ar/CC, Ar/CC/rGO$_{15}$ and Ar/CC/rGO$_{30}$ at 1.0 mV s^{-1} in H_2SO_4 1.0 Mol L^{-1}. Charge–discharge test of (c) N/CC, (d) Ar/CC, (e) N/CC/rGO$_{15}$ and (f) Ar/CC/rGO$_{15}$ at 1.5, 3.0, 6.0 and 12.0 mA for 120 s.

(**Figure 8a**) [10]. This fact represents a reduction of N_2-made electrodes specific capacitance (C_s) from 70.3 (N/CC) to 45.3 F g^{-1} (N/CC/rGO_{15}), revealing a growing capacitive current for Ar-made electrodes at same potential range from 69.6 (Ar/CC) to 197.8 F g^{-1} (Ar/CC/rGO_{15}), as maximum. Both tendencies can be associated to the micro/mesoporosity ratio (S_{micro}/S_{meso}) showed in **Table 2**, owing to the high pore free energy that restricts the ionic charge transfer in the electrode-electrolyte interface [34, 40]. Thus, a high microporosity implies a limited ionic polarization at non-faradaic conditions, and a low capacitive charge retention [41]. In addition, capacitive current can be increased if the mesoporous surface area is extended, as it has been seen for Ar-made electrodes.

According to galvanostatic charge–discharge test (GCD) [42, 43], specific capacitance (C_{GCD}) of N/CC tends to decrease while the impregnation time increases (**Figure 8c**). This fact can be associated to the microporous surface area (S_{micro}) increase, as shown in **Figure 8c** and **e**. This can also be attributed to the presence of series-resistance in the pores (IRS) [34, 40]. Particularly, C_{GCD} decreases from 178 to 162 F g^{-1} at 0.4 A g^{-1} of applied current density for N/CC and N/CC/rGO_{45}, respectively (**Table 3**). On the other hand, if the inert atmosphere is replaced by Ar flux at the same thermal treatment conditions, Ar/CC shows a capacitive current increment with the impregnation time (**Figure 8d** and **f**). For instance, Ar/CC shows a C_{GCD} of 129 F g^{-1}, while its rGO-modified electrode, Ar/CC/rGO_{15}, reports a value of 219 F g^{-1} at 0.4 A g^{-1} (**Table 3**).

A detailed analysis of the electrochemical behavior by electrochemical impedance spectroscopy (EIS) experiments and non-linear complex fitting (NLCF) of their equivalent circuits has been conducted. Nyquist diagrams show an electrolyte resistance (R_S) of 2 Ω approximately, as well as, non-ideal impedance loop for both N_2-made and Ar-made electrodes suggesting a non-ideal charge storage process at the electrochemical interface [44, 45].

Regarding to N_2-made electrodes, charge transport resistance (R_1) increases with the GO impregnation time at high frequencies range (10^4–10^2 Hz) (**Figure 9a**). NLCF shows that R_1value varies from 5.6 (N/CC) to 100.3 Ω (N/CC/rGO_{30}), as maximum. Moreover, at medium frequencies range (10^2 – 10^{-1} Hz) N/CC electrode shows an *IRS* of 6.3 *Ω*, whereas N/CC/rGO_{15} reports values of 33.6 *Ω* and N/CC/rGO_{30} present an *IRS* conformed by two circuit elements, R_2 and R_3 whose values are 125.8 *Ω* and 149.3 *Ω*, respectively. These results suggest that ionic transport resistance in the inner porous surface is increased from N/CC/rGO_{15} to N/CC/rGO_{30} as their microporosity becomes higher [46–48].

For the Nyquist diagram (**Figure 9**) the equivalent circuit was calculated, resulting in ideal capacitive element (C_1) of 4.8 x 10^{-5} for N/CC/rGO_{30}. This result can be associated to the presence of the rGO layer on the fiber surface [49]. According to the transmission line model, N/CC/rGO_{30} internal capacitances are represented by constant phase elements (Q_2, Q_3), where their behavior is related to

N_2-made samples	C_{GCD}/**F g^{-1}**	IR_{drop}/**V**	**Ar-made samples**	C_{GCD}/**F g^{-1}**	IR_{drop}/**V**
N/CC	178	0.1	Ar/CC	129	0.5
N/CC/rGO_5	157	0.1	Ar/CC/rGO_5	185	0.3
N/CC/rGO_{15}	136	0.3	Ar/CC/rGO_{15}	219	0.2
N/CC/rGO_{30}	163	0.8	Ar/CC/rGO_{30}	202	0.1
N/CC/rGO_{45}	162	0.4	Ar/CC/rGO_{45}	165	0.4

Table 3.
Double layer electrochemical capacitance by galvanostatic charge–discharge test (C_{GCD}) for N_2- and Ar-made electrodes [38].

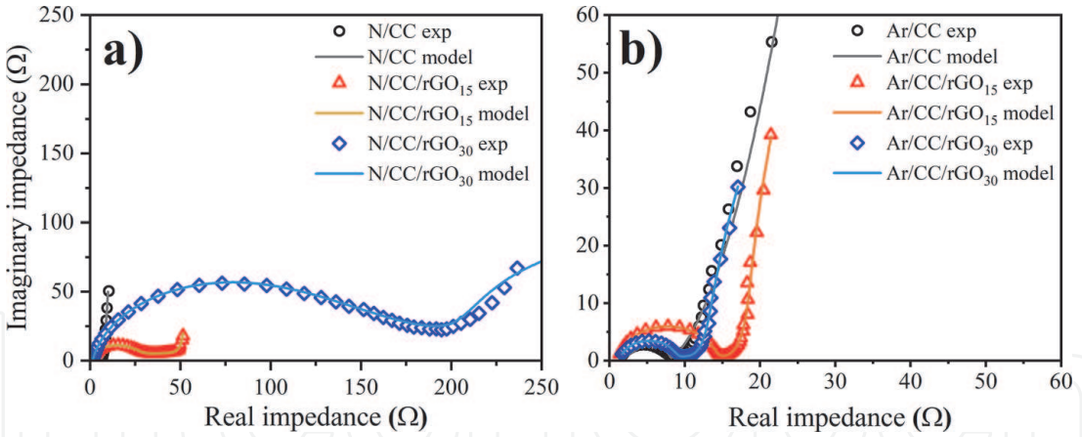

Figure 9.
Nyquist diagram of N_2-made electrodes (a) N/CC, N/CC/rGO$_{15}$ and N/CC/rGO$_{30}$ and Ar-made electrodes (b) Ar/CC, Ar/CC/rGO$_{15}$ and Ar/CC/rGO$_{30}$. Experimental (empty dots) and theoretical spectra (solid lines).

a non-ideal capacitor [44, 46]. Interestingly, the internal capacitance shows a minimum value of 0.2 Ω^{-1} $s^{\alpha 2}$ (α_2, 0,90) for N/CC/rGO$_{30}$ (**Figure 10a**) [50]. Furthermore, N/CC/rGO$_5$ and N/CC/rGO$_{45}$ show a similar correlation with the impregnation time.

Besides, Ar-made samples report lower charge transport resistance (R_1) than N_2-made electrodes. For instance, Ar/CC shows a R_1 of 5.8 Ω, while Ar/CC/rGO$_{15}$ reports a value of 2.1 and Ar/CC/rGO$_{30}$ registers a R_1 of 2.8 Ω. As well, *IRS* is represented by a unique circuit element (R_2) of 12.8 and 7.3 Ω for Ar/CC/rGO$_{15}$ and Ar/CC/rGO$_{30}$, respectively. Remarkably, Ar-made samples report a laminar mesoporosity, suggesting that ionic diffusion is controlled by the pore characteristics. Hence, a finite diffusion element (M) is used to describe the capacitive behavior at low frequencies (**Figure 10b**) [46, 47, 50]. In this sense, Ar/CC/rGO$_{15}$ presents a constant phase element (Q_3) of 0.6 Ω^{-1} $s^{\alpha 3}$ (α_3, 0.99), and a Warburg impedance (W) of 0.3 Ω^{-1} $s^{0.5}$. On the other hand, Ar/CC/rGO$_{30}$ presents a non-

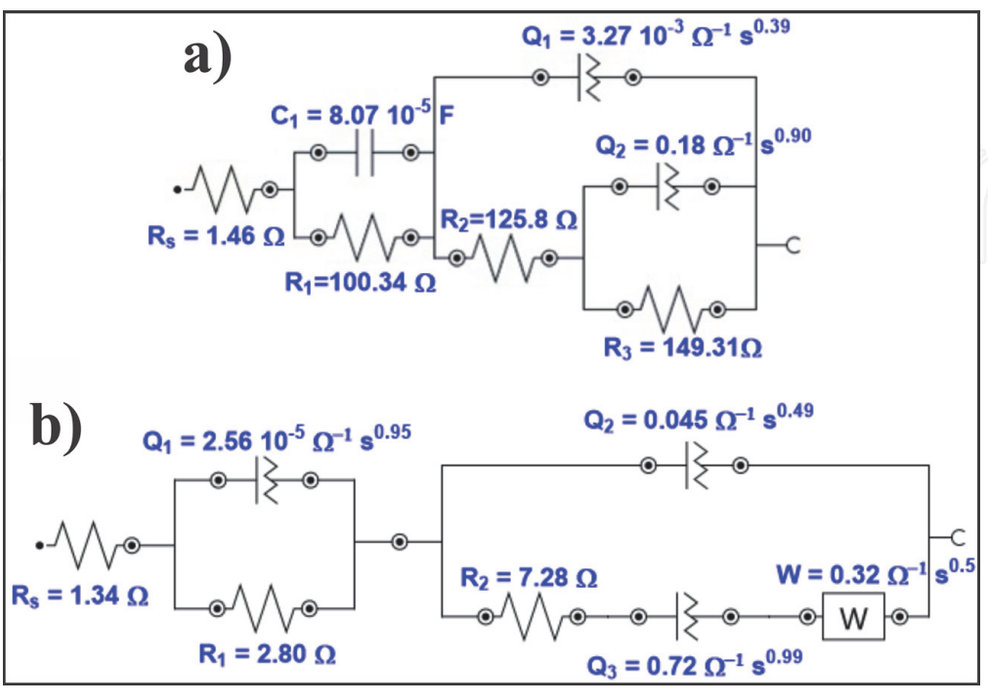

Figure 10.
Equivalent circuit of (a) N/CC/rGO$_{30}$, (b)Ar/CC/rGO$_{30}$. The inserted values are calculated from non-linear complex fitting of the EIS measurements.

ideal capacitance of Q_3 of 0.7 $\Omega^{-1} s^{\alpha 3}$ (α_3, 0.99) together to diffusion impedance W of 0.3 $\Omega^{-1} s^{0.5}$ (**Figure 10b**). In contrast, Ar/CC only shows an ideal capacitive behavior of 3.0 x 10^{-5} F (C_{dl}) and internal one of 0.2 F.

Accordingly, the total capacity (C_{EIS}) from the internal capacitive element (Q^{α}_{EIS}) is reported where the non-ideal constant (α) tends to one. For the estimation of the electrochemically accessible surface (S_{EIS}), a double layer charge density (Q^{o}_{dl}) of glassy carbon electrode of 3.0 x 10^{-5} F cm^{-2} is considered [51, 52],

$$S_{EIS}\left(m^2 g^{-1}\right) = Q_{EIS}^{\alpha \approx 1.0} / \left(mxQ^{o}_{dl}\right) \quad (6)$$

Additionally, the electrochemically accessible surface ratio (R_{ESA}) registers the fraction of interface surfaces available in the total physical surface area (S_{BET}) [52].

$$R_{ESA} = S_{EIS}/S_{BET} \quad (7)$$

The difference between C_{EIS} and C_{GCD} values show the total charge related to the electrochemical double layer, whereas the GCD test also registers the faradaic charge caused by the surface carbon and oxygen groups [52, 53]. As we can observe in **Table 4**, N_2-made samples present a decrease of the R_{ESA} (from 0.6 to 0.2) which can be related to the increment of the free energy adsorption promoted by their microporosity. The opposite occurs in Ar-made electrodes where R_{ESA} increases (from 0.2 to 0.4) and it can be related to their laminar mesoporous surface which results in a controlled ionic diffusion. Based on the R_{ESA} results, Ar/CC/rGO_{15} and Ar/CC/rGO_{30} electrodes emerge as promising candidates for the design of supercapacitors.

The aforementioned results enable us to conclude that the inert atmosphere has a strong influence on the surface and electrochemical characteristics of the synthetized carbon-based electrodes. Under N_2 atmosphere, N/CC and N/CC/$rGO_{5\text{-}45}$ show a remarkable microporous surface area. Unfortunately, this high microporosity affects the ionic diffusion, capacitive behavior and resistive character. Otherwise, under Ar atmosphere, an increase of the mesoporous surface is reported, based on a laminar pore distribution, associated with controlled ionic diffusion in the electrochemical cell, resulting in an increase of the capacitance.

Samples		C_{GCD}/ F g^{-1}	$Q_{EIS}^{\alpha \approx 1.0}$/ F	C_{EIS}/ F g^{-1}	S_{EIS}/ m^2 g^{-1}	S_{BET}/ m^2 g^{-1}	R_{ESA}
N_2-made electrodes	N/CC	178	0.3	85	285	453	0.6
	N/CC/rGO_5	157	0.2	60	198	—	—
	N/CC/rGO_{15}	136	1.0	112	373	1221	0.3
	N/CC/rGO_{30}	163	0.2	94	315	1805	0.2
	N/CC/rGO_{45}	162	0.3	57	191	—	—
Ar-made electrodes	Ar/CC	129	0.2	64	212	1074	0.2
	Ar/CC/rGO_5	185	0.4	108	359	—	—
	Ar/CC/rGO_{15}	219	0.6	172	573	1458	0.4
	Ar/CC/rGO_{30}	202	0.7	149	497	1207	0.4
	Ar/CC/rGO_{45}	165	0.3	111	369	—	—

Table 4.
Comparative chart between double layer electrochemical performance and superficial characteristics for N_2- and Ar-made carbon-based electrodes [38].

Remarkably, both Ar/CC/rGO_{15} and Ar/CC/rGO_{30} exhibit a promising capacitive behavior, as well as an optimal electrochemical accessible surface.

In this sense, the design of carbon-based electrodes from biomass-derived materials represents an outstanding way to obtain several energy-store electrochemical systems [54–56]. In addition, a remarkable capacity retention depending on pore size distribution looks like a constant effect on the constitution of double layer interface (DLI).

For instance, L. Jiang et al., reported a high performance of cellulose-derived microporous electrodes of 115 F g^{-1} and > 87% of capacity retention [54]. As well, Y. Zou et al., described rGO-intercalated carbon cloth fibers electrodes with a meso/micro-porous distribution and 64.5 mF cm^{-2} of specific capacitance [55]. Sheng-Heng C. et al. show that macro/micro-porosity to carbonized cotton fibers produce carbons with notable surface area [56]. On the other hand, Hui Shao et al., have paid special attention to nanoscale pores on carbon materials obtained by templates and double layer capacitance behavior at inside of this nanoscale pores [57]. Therefore, this fact is still discussed, owing to non-clear description is achieved by a cylindrical pore model in overall cases. Other parameters as the kind of inert atmosphere are considered in this work. Herein, a brief explanation of porosity-electrochemical performance is described, and inert atmosphere influence has been exposed as a significant parameter, as well as gas flux and temperature, certainly [38, 39].

Acknowledgements

The authors wish to thank the Vice-Rectorate of Research of National University of Engineering (UNI), Contract P-CC-2021-000546, and the Peruvian government agencies CONCYTEC and FONDECYT /World Bank (ref. 026-2019 FONDECYT-BM-INC.INV).

Conflict of interest

The authors declare no 'conflict of interest'.

Author details

Antony Bazan-Aguilar[1], Elvis O. López[2], Miguel Ponce-Vargas[3] and Angélica M. Baena-Moncada[1*]

1 Research Laboratory in Applied Electrochemical, National University of Engineering (UNI), Lima, Peru

2 Department of Experimental Low Energy Physics, Brazilian Center for Research in Physics (CBPF), Rio de Janeiro, Brazil

3 Institut de Chimie Moléculaire de Reims UMR CNRS 7312, Université de Reims Champagne-Ardenne, Reims, France

*Address all correspondence to: abaenam@uni.edu.pe

References

[1] Nejat P, Jomehzadeh F, Taheri MM, Gohari M, Abd. Majid MZ. A global review of energy consumption, CO2 emissions and policy in the residential sector (with an overview of the top ten CO2 emitting countries). Renew Sustain Energy Rev. 2015;43:843–62.

[2] Oncel SS. Green energy engineering: Opening a green way for the future. J Clean Prod. 2017;142:3095–100.

[3] Viviescas C, Lima L, Diuana FA, Vasquez E, Ludovique C, Silva GN, et al. Contribution of Variable Renewable Energy to increase energy security in Latin America: Complementarity and climate change impacts on wind and solar resources. Renew Sustain Energy Rev. 2019 Oct;113:109232.

[4] Gao Z, Zhang Y, Song N, Li X. Biomass-derived renewable carbon materials for electrochemical energy storage. Mater Res Lett. 2017 Mar;5(2): 69–88.

[5] Meng Q, Cai K, Chen Y, Chen L. Research progress on conducting polymer based supercapacitor electrode materials. Nano Energy. 2017;36 (February):268–85.

[6] Wang J, Zhang X, Li Z, Ma Y, Ma L. Recent progress of biomass-derived carbon materials for supercapacitors. J Power Sources. 2020;451(January): 227794.

[7] Han X, Lu L, Zheng Y, Feng X, Li Z, Li J, et al. A review on the key issues of the lithium ion battery degradation among the whole life cycle. eTransportation. 2019 Aug;1:100005.

[8] Wentker M, Greenwood M, Asaba MC, Leker J. A raw material criticality and environmental impact assessment of state-of-the-art and post-lithium-ion cathode technologies. J Energy Storage. 2019 Dec;26:101022.

[9] Afif A, Rahman SM, Tasfiah Azad A, Zaini J, Islan MA, Azad AK. Advanced materials and technologies for hybrid supercapacitors for energy storage – A review. J Energy Storage. 2019;25(July): 100852.

[10] Gogotsi Y, Penner RM. Energy Storage in Nanomaterials - Capacitive, Pseudocapacitive, or Battery-like? ACS Nano. 2018;12(3):2081–3.

[11] Wang Y, Lei Y, Li J, Gu L, Yuan H, Xiao D. Synthesis of 3D-nanonet hollow structured Co3O4 for high capacity supercapacitor. ACS Appl Mater Interfaces. 2014;6(9):6739–47.

[12] Muzaffar A, Ahamed MB, Deshmukh K, Thirumalai J. A review on recent advances in hybrid supercapacitors: Design, fabrication and applications. Renew Sustain Energy Rev. 2019;101(October 2018):123–45.

[13] Frackowiak E, Abbas Q, Béguin F. Carbon/carbon supercapacitors. J Energy Chem. 2013;22(2):226–40.

[14] Li X, Wei B. Supercapacitors based on nanostructured carbon. Nano Energy. 2013;2(2):159–73.

[15] Simon Patrice, Brousse Thierry FF. Supercapacitors Based on Carbon or Pseudocapacitive Materials. 2017. 1–122 p.

[16] Zheng C, Qian W, Cui C, Xu G, Zhao M, Tian G, et al. Carbon nanotubes for supercapacitors: Consideration of cost and chemical vapor deposition techniques. J Nat Gas Chem. 2012;21(3): 233–40.

[17] Zhang Qing RK. Synthesis of Garlic Skin-Derived 3D Hierarchical Porous Carbon for High-Performance Supercapacitors. Nanoscale. 2018;1–9.

[18] Zhang G, Chen Y, Chen Y, Guo H. Activated biomass carbon made from bamboo as electrode material for supercapacitors. Mater Res Bull. 2018; 102(2010):391–8.

[19] Kumagai S, Sato M, Tashima D. Electrical double-layer capacitance of micro-and mesoporous activated carbon prepared from rice husk and beet sugar. Electrochim Acta. 2013;114:617–26.

[20] Yadav N, Ritu R, Promila P, Hashmi SA. Hierarchical porous carbon derived from eucalyptus-bark as a sustainable electrode for high-performance solid-state supercapacitors. Sustain Energy Fuels. 2020;7–35.

[21] Xu X, Zhou J, Jiang L, Lubineau G, Chen Y, Wu X-F, et al. Porous core-shell carbon fibers derived from lignin and cellulose nanofibrils. Mater Lett. 2013; 109:175–8.

[22] Wan L, Chen D, Liu J, Zhang Y, Chen J, Du C, et al. Facile preparation of porous carbons derived from orange peel via basic copper carbonate activation for supercapacitors. J Alloys Compd. 2020;823:153747.

[23] Elmouwahidi A, Bailón-García E, Pérez-Cadenas AF, Carrasco-Marín F. Valorization of agricultural wood wastes as electrodes for electrochemical capacitors by chemical activation with H_3PO_4 and KOH. Wood Sci Technol. 2020;54(2):401–20.

[24] Yu M, Han Y, Li J, Wang L. CO2-activated porous carbon derived from cattail biomass for removal of malachite green dye and application as supercapacitors. Chem Eng J. 2017;317: 493–502.

[25] Veerakumar P, Sangili A, Manavalan S, Thanasekaran P, Lin K-C. Research Progress on Porous Carbon Supported Metal/Metal Oxide Nanomaterials for Supercapacitor Electrode Applications. Ind Eng Chem Res. 2020;

[26] Wang J, Kaskel S. KOH activation of carbon-based materials for energy storage. J Mater Chem. 2012;22(45): 23710–25.

[27] Barzegar F, Khaleed AA, Ugbo FU, Oyeniran KO, Momodu DY, Bello A, et al. Cycling and floating performance of symmetric supercapacitor derived from coconut shell biomass. AIP Adv. 2016;6(11).

[28] Yin L, Chen Y, Li D, Zhao X, Hou B, Cao B. 3-Dimensional hierarchical porous activated carbon derived from coconut fibers with high-rate performance for symmetric supercapacitors. Mater Des. 2016;111: 44–50.

[29] Sesuk T, Tammawat P, Jivaganont P, Somton K, Limthongkul P, Kobsiriphat W. Activated carbon derived from coconut coir pith as high performance supercapacitor electrode material. J Energy Storage. 2019;25 (June):100910.

[30] Andreas HA, Conway BE. Examination of the double-layer capacitance of an high specific-area C-cloth electrode as titrated from acidic to alkaline pHs. Electrochim Acta. 2006;51 (28):6510–20.

[31] Wang H, Chen Z, Liu HK, Guo Z. A facile synthesis approach to micro–macroporous carbon from cotton and its application in the lithium–sulfur battery. RSC Adv [Internet]. 2014;4 (110):65074–80. Available from: http://xlink.rsc.org/?DOI=C4RA12260G

[32] Rhim YR, Zhang D, Fairbrother DH, Wepasnick KA, Livi KJ, Bodnar RJ, et al. Changes in electrical and microstructural properties of microcrystalline cellulose as function of carbonization temperature. Carbon N Y [Internet]. 2010;48(4):1012–24.

Available from: http://dx.doi.org/10.1016/j.carbon.2009.11.020

[33] Chung SH, Chang CH, Manthiram A. A Carbon-Cotton Cathode with Ultrahigh-Loading Capability for Statically and Dynamically Stable Lithium-Sulfur Batteries. ACS Nano. 2016;10(11): 10462–70.

[34] Chen L, Ji T, Mu L, Zhu J. Cotton fabric derived hierarchically porous carbon and nitrogen doping for sustainable capacitor electrode. Carbon N Y [Internet]. 2017;111:839–48. Available from: http://dx.doi.org/10.1016/j.carbon.2016.10.054

[35] Fan L-Z, Chen T-T, Song W-L, Li X, Zhang S. High nitrogen-containing cotton derived 3D porous carbon frameworks for high-performance supercapacitors. Sci Rep [Internet]. 2015;5(August):15388. Available from: http://www.nature.com/articles/srep15388

[36] Zhang X, Huang X, Zhang X, Zhong B, Xia L, Liu J, et al. A facile method to prepare graphene-coat cotton and its application for lithium battery. J Solid State Electrochem. 2016;20(5): 1251–61.

[37] Tang M., Bacon R. Carbonization of cellulose fibers—I. Low temperature pyrolysis. Carbon N Y. 1964;2(3):211–20.

[38] Bazan-Aguilar A, Ponce-Vargas M, Caycho CL, La Rosa-Toro A, Baena-Moncada AM. Highly Porous Reduced Graphene Oxide-Coated Carbonized Cotton Fibers as Supercapacitor Electrodes. ACS Omega [Internet]. 2020 Dec 22;5(50):32149–59. Available from: https://doi.org/10.1021/acsomega.0c02370

[39] Bazan A. Estudio Espectroscópico y Morfológico en el Grafeno. Universidad Nacional de Ingenieria; 2016.

[40] Zou Y, Wang S. Interconnecting carbon fibers with the in-situ electrochemically exfoliated graphene as advanced binder-free electrode materials for flexible supercapacitor. Sci Rep [Internet]. 2015;5(July):1–7. Available from: http://dx.doi.org/10.1038/srep11792

[41] Wang Y, Song Y, Xia Y. Electrochemical capacitors: mechanism, materials, systems, characterization and applications. Chem Soc Rev [Internet]. 2016;45:5925–50. Available from: http://dx.doi.org/10.1039/C5CS00580A

[42] Jiang L, Nelson GW, Kim H, Sim IN, Han SO, Foord JS. Cellulose-Derived Supercapacitors from the Carbonisation of Filter Paper. ChemistryOpen. 2015;4(5):586–9.

[43] Abushrenta N, Wu X, Wang J, Liu J, Sun X. Hierarchical Co-based Porous Layered Double Hydroxide Arrays Derived via Alkali Etching for High-performance Supercapacitors. Sci Rep [Internet]. 2015;5(July):1–9. Available from: http://dx.doi.org/10.1038/srep13082

[44] Barsoukov E, Macdonald JR. Impedance Spectroscopy [Internet]. Impedance Spectroscopy: Theory, Experiment, and Applications. 2005. 1–595 p. Available from: http://doi.wiley.com/10.1002/0471716243

[45] Hasyim MR, Ma D, Rajagopalan R, Randall C. Prediction of Charge-Discharge and Impedance Characteristics of Electric Double-Layer Capacitors Using Porous Electrode Theory. J Electrochem Soc. 2017;164(13):A2899–913.

[46] Klink S. In-depth analysis of irreversible processes in lithium ion batteries. Ruhr-Universität Bochum, Universitätsbibliothek; 2013.

[47] Newman JS, Tobias CW. Theoretical Analysis of Current

Distribution in Porous Electrodes. J Electrochem Soc. 2007;109(12):1183.

[48] ZIVE-Lab. ZMAN 2.3.2 User's Manual. ZIVE-Lab W, editor. Seoul, Korea: WonATech Co., Ltd; 2014. 1–173 p.

[49] Yang C. Reduced Graphene Oxide–Based Microsupercapacitors. In: Jiang Z, Kyzas G, editors. Rijeka: InTech; 2017. p. Ch. 6. Available from: https://doi.org/10.5772/67433

[50] Kang J, Wen J, Jayaram SH, Yu A, Wang X. Development of an equivalent circuit model for electrochemical double layer capacitors (EDLCs) with distinct electrolytes. Electrochim Acta [Internet]. 2014;115:587–98. Available from: http://dx.doi.org/10.1016/j.electacta.2013.11.002

[51] Fernández PS, Castro EB, Real SG, Visintin A, Arenillas A, Calvo EG, et al. Electrochemical behavior and capacitance properties of carbon xerogel/multiwalled carbon nanotubes composites. J Solid State Electrochem. 2012;16(3):1067–76.

[52] Fernández PS, Arenillas A, Calvo EG, Menéndez JA, Martins ME. Carbon xerogels as electrochemical supercapacitors. Relation between impedance physicochemical parameters and electrochemical behaviour. Int J Hydrogen Energy. 2012;37(13): 10249–55.

[53] Martin R, Quintana JJ, Ramos A, Nuez I De. Modeling Electrochemical Double Layer Capacitor , from Classical to Fractional Impedance. 2008;61–6.

[54] Luyun Jiang, Geoffrey W. Nelson, Heeyeon Kim, I. N. Sim, Seong Ok Han, and John S. Foord. Cellulose-Derived Supercapacitors from the Carbonisation of Filter Paper. ChemistryOpen 2015, 4, 586–589. DOI: 10.1002/open.201500150.

[55] Yuqin Zou, Shuangyin Wang. Interconnecting Carbon Fibers with the In-situ Electrochemically Exfoliated Graphene as Advanced Binder-free Electrode Materials for Flexible Supercapacitor. Scientific RepoRts. 5: 11792. DOi: 10.1038/srep11792.

[56] Sheng-Heng Chung, Chi-Hao Chang, Arumugam Manthiram. A Carbon-Cotton Cathode with Ultrahigh Loading Capability for Statically and Dynamically Stable Lithium−Sulfur Batteries. ACS Nano 2016, 10, 11, 10462–10470

[57] Hui Shao, Yih-Chyng Wu, Zifeng Lin, Pierre-Louis Taberna, Patrice Simon. Nanoporous carbon for electrochemical capacitive energy storage. Chem. Soc. Rev., 2020, 49, 3005. DOI: 10.1039/d0cs00059k